DETECTION OF WAVES IN THE EQUATORIAL CORONAL HOLES

D. Banerjee[1], E. O'Shea[2], and J.G. Doyle[2]

[1]*Indian Institute of Astrophysics, Koramangala, Bangalore 560034, India*
[2]*Armagh Observatory, College Hill, Armagh BT61 9DG, N. Ireland*

ABSTRACT

We examine long spectral time series of coronal holes with the Coronal Diagnostic Spectrometer (CDS) onboard SoHO. The observations were obtained with several transition region and coronal lines. We compare the dynamics of equatorial coronal holes and the polar coronal holes. Presence of long period waves in the plumes and inter-plume regions have been reported earlier from CDS and SUMER observations. From a study of several transition region and coronal lines we will report on the presence of long period outwardly propagating waves in several locations on the disk part of the coronal holes. From a joint study of SUMER and MDI, recently it has been discovered that the fast solar wind originates from the coronal funnels in the polar regions. In this presentation we will focus on the equatorial coronal holes. We will also try to search for the origin of these long period waves and will report on the connection, if any, of network boundaries in the coronal holes. If we are able to identify and characterize these waves properly, they will provide additional tools in the study of coronal seismology.

Key words: Sun: Corona: Oscillations: coronal hole: Waves.

1. INTRODUCTION

Coronal holes (Munro and Withbroe, 1972) are "dark" coronal regions of the Sun with open magnetic field structure. During the minimum years of the solar cycle they are confined in the Sun's polar regions, while at solar maximum they can be found at all latitudes. The fast-speed solar wind originates form the coronal holes (e.g., Krieger et al., 1973), and accordingly they are considered the main reason for the "recurrent" type of geomagnetic activity. Evidence for waves in the outer atmosphere of the Sun comes from measurements of radiance and Doppler velocity oscillations in a range of frequencies, including visible, ultraviolet, X-ray and radio, given off by different solar structures at chromospheric, transition region and coronal temperatures. A number of studies Ofman et al. (1997), DeForest & Gurman (1998), Banerjee et al. (2000), Banerjee et al. (2001a,b), have measured oscillations in plumes, interplumes and coronal holes in the polar regions of the Sun. All of these studies point to the presence of compressional waves, thought to be slow magnetoacoustic waves as found by DeForest & Gurman (1998).

Table 1. A log of the datasets.

Date	Dataset	Region	Start time
07/12/02	26412r00	Equatorial CH	12:22
07/12/02	26412r01	Equatorial CH	15:13
10/12/02	26431r00	Equatorial CH	16:26
10/12/02	26431r01	Equatorial CH	19:17
11/12/02	26435r00	North polar CH	06:33
20/12/02	26502r00	South polar CH	18:00
20/12/02	26502r01	South polar CH	20:50

2. OBSERVATIONS AND DATA REDUCTION

For these observations we have used the normal incidence spectrometer (NIS), which is one of the components of the Coronal Diagnostic Spectrometer (CDS) on board the Solar and Heliospheric Observatory (SOHO), see Harrison et al. (1995). The temporal series SER150W sequence was run during December 2002 in the coronal hole region, with equatorial coronal hole and the north and the Southern polar coronal hole region (see Table 1). Fig. 1 shows the slit locations for the CDS datasets, over-plotted on EIT 284 images (Log T$\approx 2\times10^6$K) which were observed at times approximate to those of the CDS datasets. Data was obtained for 11 transition region and coronal lines. However, here we shall only discuss four of these; the transition region line of O v 629.73 Å ($\approx 2.5\times10^5$ K) and the coronal lines of Mg x

Proceedings of the International Scientific Conference on Chromospheric and Coronal Magnetic Fields, 30 August – 2 September 2005 (ESA SP-596, November 2005)

609.79, 624.94 Å ($\approx 1.25\times10^6$ K) and Si XII 520.67 Å ($\approx 2.5\times10^6$ K). Note that we shall henceforth refer to the lines without the following decimal places, e.g., 629 in place of 629.73. The data was reduced using the latest versions of the standard CDS routines[1]. Before fitting the lines with a single Gaussian, and in order to increase the signal-to-noise ratio, we binned by 2 along the 143 pixel slit to produce 70 usable pixels ($4''\times3.36''$) in Y.

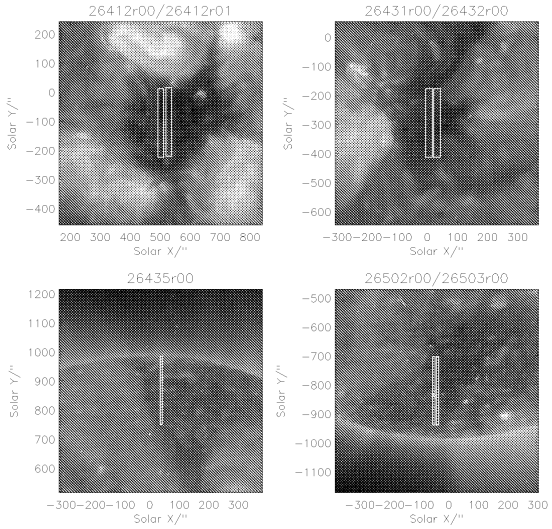

Figure 1. (Top left) EIT 284 image taken at 13:06 UTC on 7/12/02 showing the total area traversed by the 26412r00 (on the left) and the 26412r01 slit (on the right) during the period of the observations. (Top right) EIT 171 image taken at 19:06 UTC on 10/12/02 showing the area traversed by the 26431r00 slit (on the right) and the 26432r00 slit (on the left).(Bottom left) EIT 171 image taken at 07:06 UTC on the 11/12/02 showing the area traversed by the 26435r00 slit. (Bottom right) EIT 171 image taken at 19:06 UTC on the 20/12/02 showing the area traversed by the 26502r00 slit (on the right) and 26503r00 (on the left).

3. RESULTS

3.1. Polar coronal hole regions

In Fig. 1 (lower right panel) one can find the location of the slit corresponding to dataset, s26502/s26503, taken in a south polar coronal hole, as observed on 20th December. In Fig. 2 we show the space time behaviour of a portion of the slit as observed by different temperature lines, in the form of X-T slices (the grey scale panels). To bring out the details of the original intensity map (X-T slice) we have filtered out the high frequency components in the image (see Doyle et al. 1999 for details). In this contrast enhanced image, the solar north-south (SOLAR_Y) direction is in the vertical axis, the horizontal axis is time.

[1] http://solg2.bnsc.rl.ac.uk/software/uguide/uguide.shtml

The right panels show the total number of counts in a pixel. The grey scale coding has the most intense regions as white. The alternate bright and dark ridges indicate the presence of oscillations in intensity. In Fig. 3 we show the same region as seen from EIT. Note the location of the brightening in both the figures (around px26).

Next, we show the spatial behaviour of the oscillation frequencies measured from the different temperature lines in Fig. 4 for the same portion of the slit. These figures show the measured frequencies as a function of position along the slit (X-f slice). The circles and the plus symbols correspond to the primary maxima and the secondary maxima in the global wavelet power spectra, which have a probability of more than the 95% after the randomisation test. The total number of counts in a pixel (summed counts) during the observation is shown in the right column, and is useful in identifying bright locations and network boundaries within the coronal hole (pixel 26 corresponds to the bright point). The intensity results show that the primary maxima in the global wavelet spectra lies in the range 0.5-1.0 mHz. The appearance of more points in the intensity X-f slices of O V as compared Mg X also indicates that the intensity oscillations are stronger and more reliable ($>$ 95% probability level) in the case of the transition region line. But is could be also an indication that whatever causes these oscillations they are present everywhere in the transition region but as far as the coronal regions are concerned they seem to be present around the bright point.

Now we present in Fig 5 the wavelet results for intensity in different temperature lines, corresponding to a single pixel (px 26) the bright one, within the coronal hole as recorded in the s26503 dataset. We should point out here that the velocity signal is often weak for the coronal lines in a single pixel and the resulting oscillations are most of the time not significant. Thus we do not show plots for velocity power in this short contribution. The intensity variations are shown in the top panels. In the wavelet spectrum the dark contour regions show the locations of the highest power. The light white horizontal lines within the dark contour regions indicate the locations of the maximum wavelet power at each particular time. The lowest panel shows the variation of the probability level over the observing time, by which it is possible to see whether the maximum wavelet power at any time in the wavelet spectrum has a high or low probability of being due to noise. Only locations that have a probability greater than 95% are regarded as being real, *i.e.* not due to noise. Cross-hatched regions, on either side of the wavelet spectrum, indicate the 'cone of influence' (COI), where edge effects become important (see Torrence & Compo, 1998).

3.2. Equatorial coronal hole regions

Now, we turn our attention to a dataset s26431 and s26432, which was taken within an equatorial coronal hole (see Table 1). We just randomly look at any single

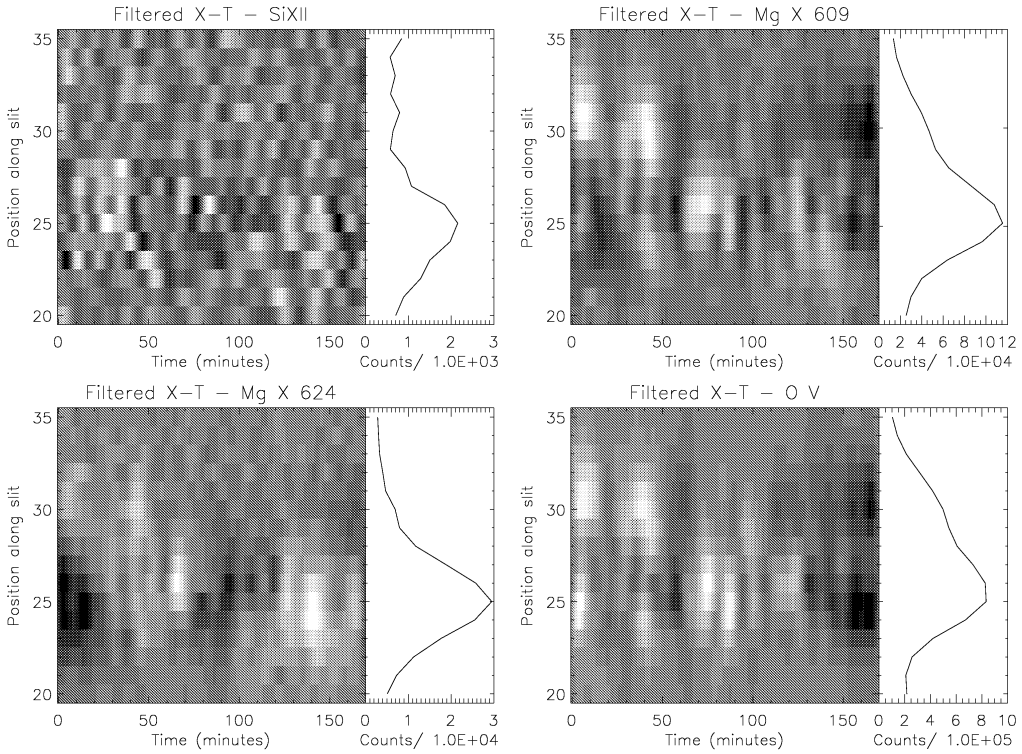

Figure 2. Space time behaviour of different temperature lines (X-T slice), for dataset s26503, in the South polar coronal hole.

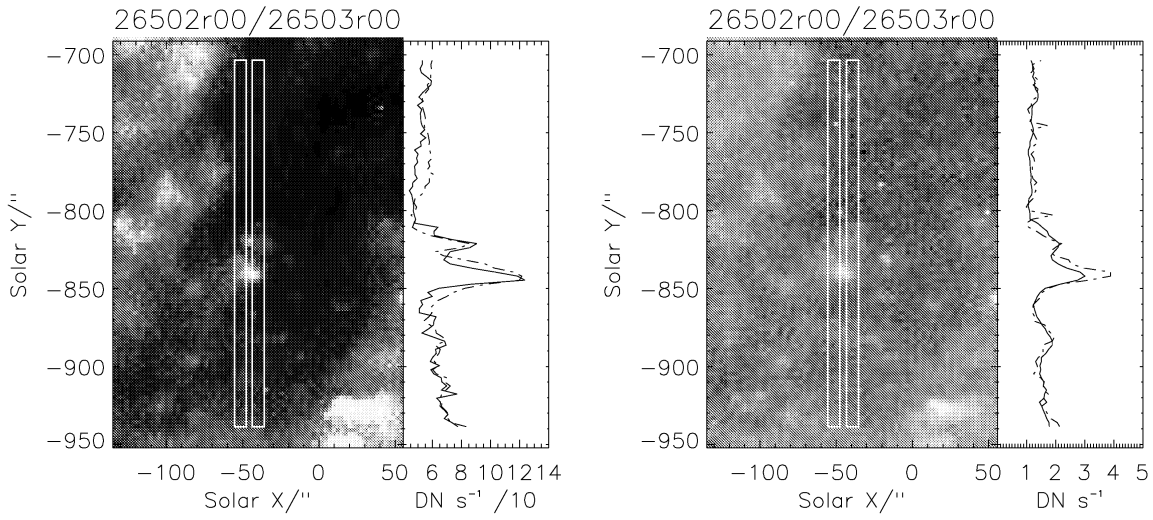

Figure 3. (Top left) Close-up of the EIT 171 images of 20/12/02 showing the area traversed by the 26502 slit (right) and the 26503 slit (left). On the right is shown the variation along Solar Y of the summed EIT intensity within the area traversed by the 26502 slit (solid line) and the 26503r00 slit (dot-dashed line). The summed intensity is shown in EIT units of Data Numbers (DN) s^{-1}. The right set of panels correspond to EIT 284 image with same representation.

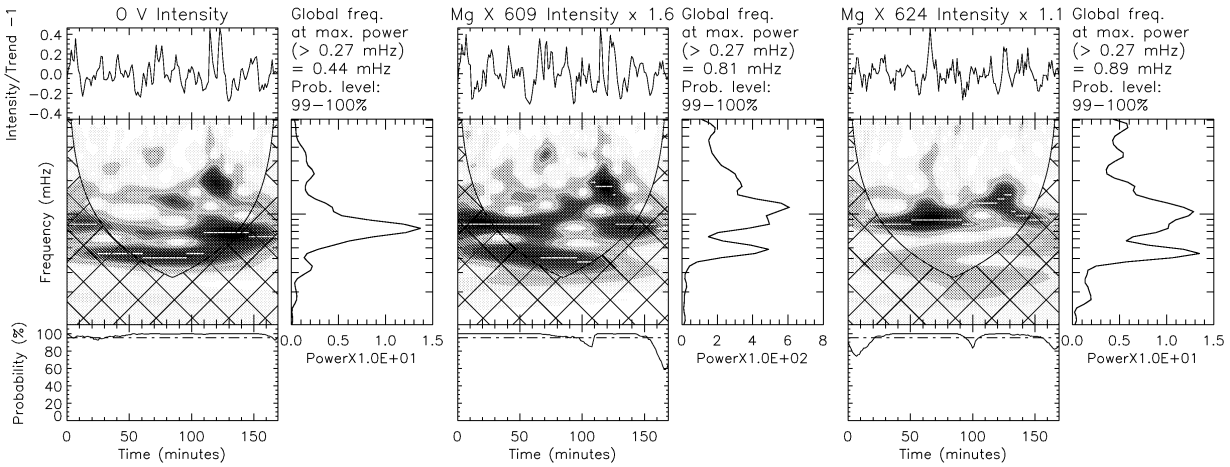

Figure 5. Intensity wavelet results corresponding to the s26503 dataset taken in the south polar coronal hole and corresponding to the pixel location 26.

pixel, e.g. px8 and plot the wavelet results in Fig 6. The transition region line O v and the other coronal lines, all show significant oscillations within 0.7-0.9 mHz. The oscillations shown in Fig. 6 have had their background trend removed by dividing the original time series by a 25-point running average (i.e.,a ≈28 min interval). We produce the relative intensities shown in the plot by then subtracting a value of one from this trend removed time series. Each of the time series is shown with error bars representing the uncertainties in the radiance estimates for each of the lines. Above the global wavelet spectrum of each line in Fig. 6 are shown the frequencies measured from the first and second maxima in this global wavelet spectrum, together with estimates of probability that these oscillations are not due to noise. These probability estimates were calculated using the randomisation method as outlined in O'Sheaet al. (2001), with 250 permutations.

3.3. Phase-delay analysis

It is clear from these measured frequencies that the different lines share common oscillations, each of the lines showing the presence of an oscillation at ≈0.7 mHz as either the first or second maximum. The shape of the wavelet power spectrum in the central panels is also similar for each line. Below the wavelet power spectrum, in the lower panels, we show the variation of the probability estimate, again calculated using the randomisation technique, associated with the maximum power at each time in the wavelet power spectrum (marked with the white lines in the plot). The shared oscillations between lines

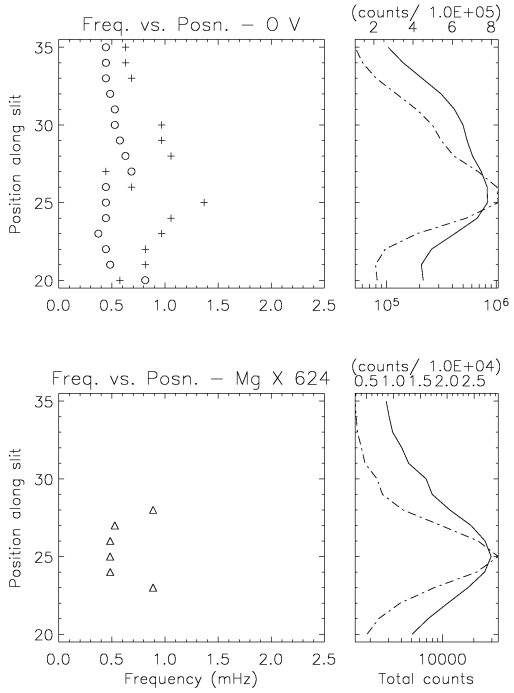

Figure 4. For dataset s26303, south polar coronal hole, spatial variation of frequency corresponding to different temperature lines, X-f slices for intensity.

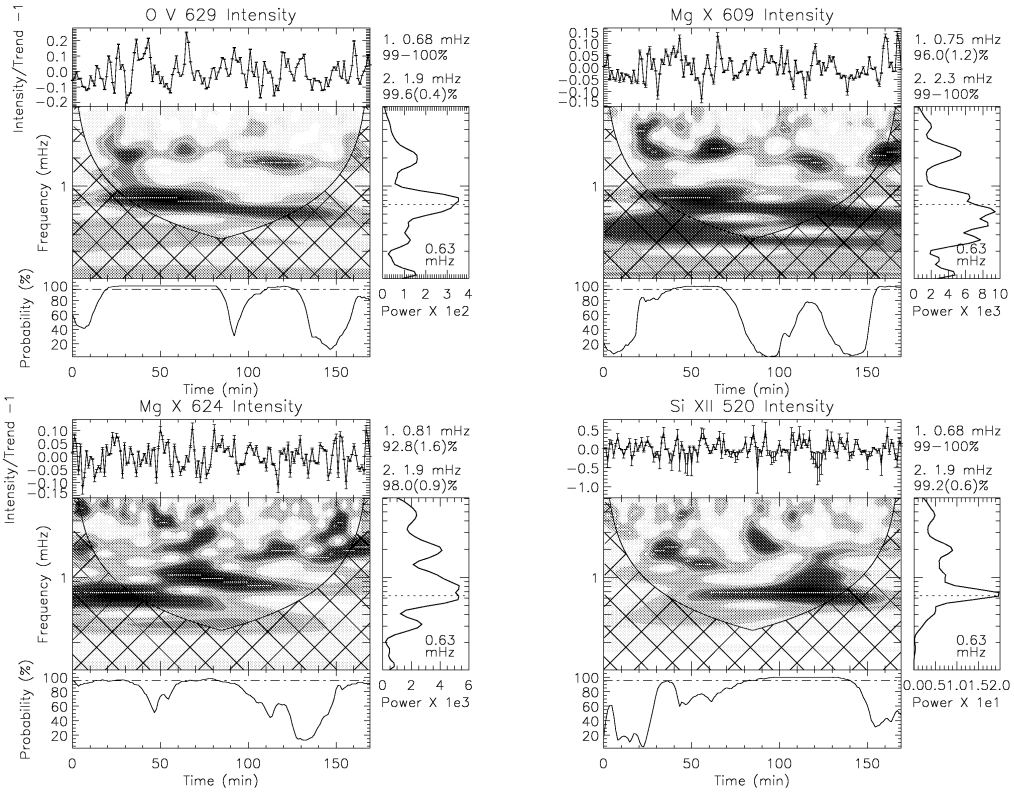

Figure 6. Intensity wavelet results for pixel location 8, within an equatorial coronal hole, corresponding to the dataset s26431.

separated by large ranges of temperature suggests that there is a link between the cooler transition line of O V and the hotter coronal line of Mg X. We suggest that the reason for the shared oscillations between these lines is due to waves propagating between the different temperature regions where these lines form. To investigate this we measured the phase delays in flux and line-of-sight (LOS) velocity between different line pairs. To calculate the phase delays we used standard Fourier analysis techniques, following closely the 'recipe' given in Appendix A of Doyle et al. (1999). Phase delays were calculated using confidence levels of 95 and 99%, that is, only those measured phase values with a squared coherency spectral estimate above these levels were selected. Over-plotted on some of the circle symbols in Fig. 7 are representative error bars showing average uncertainties in the phase delay calculations at the 95 and 99% significance levels. Phase delays measured at the 99% significance level are shown as the larger circles.

Note that in this work we follow the treatment used by Athay & White (1979) in which the calculated phase delays are plotted over the full -180 to $+180$ degree (360 degree) range and as a function of measured oscillation frequency. Since the expected phase difference is given by $\Delta\phi$=$2\pi fT$, where f is the frequency and T the time delay in seconds, the phase difference will vary linearly with f, and will change by 360 degree over frequency intervals of Δf=$1/T$. This will give rise to parallel lines in the $\Delta\phi$ vs. f plots at fixed frequency intervals (Δf=$1/T$) corresponding to the fixed time delay T. The details of this analysis can be found in O'Shea et al. (2005). The results of our phase delay analysis is shown in Fig. 7. For the Equatorial coronal hole region, corresponding to the dataset, 26431, 26432 we find fixed time-delay of 167s (which is measured from the slopes of those fitted slanted lines). Now we have estimated the formation height difference of 8937 Km between O V and Mg X (see O'Shea et al. 2005 for details), which yields the propagation speed $\approx$ 54 km/s. On the other hand for the south polar coronal hole we find the fixed time-delay $\approx$ 100s, which corresponds to a phase speed of 89 km/s.

4. CONCLUSION

In the present study, from simultaneous measurements of oscillations at transition region and coronal temperatures, evidence is found for outwardly propagating waves in the coronal hole regions. We find a possible link of the bright points as a source of these oscillations. Measurements of phase delays between these oscillations provides evidence of fixed time delays between the measured transition region-coronal O V 629–Mg X 624 line pair. By estimating the formation heights of the different lines we estimate propagation speeds for the different line pairs that

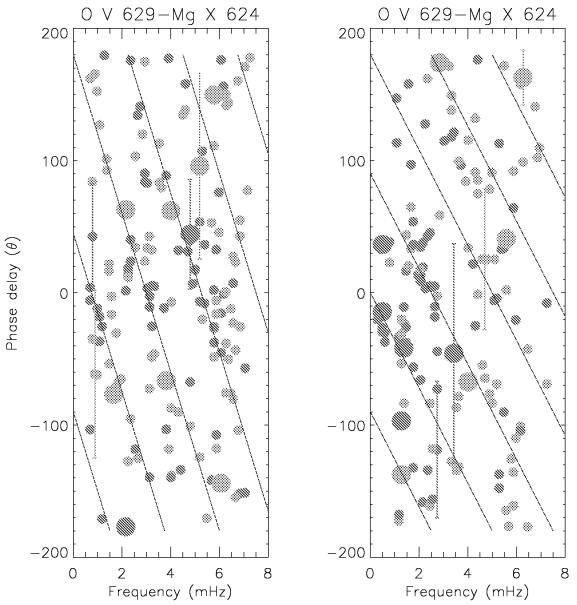

Figure 7. Phase delays measured between the oscillations in the different line pairs corresponding to the equatorial coronal hole and the s26431 and s 26432 dataset (left panel) and the south polar coronal hole, the s26502 and s26503 dataset (right panel). Radiance oscillations are shown as the orange circles while L.O.S. velocity oscillations are shown as the green circles. Phase delays were measured at the 95% and 99% significance levels. Phase delays at the 99% significance level are indicated by the slightly larger symbols. Average uncertainties in the 95% and 99% phase delay estimates are shown by the representative error bars in each plot. Over-plotted on this plot are lines corresponding to fixed time delays.

indicates that the waves producing the observed phase delays are magnetoacoustic waves propagating close to the sound speed. From the above discussion we can conclude that these waves are slow mode magnetoacoustic waves. We also find an indication that the phase speed is lower in the equatorial coronal hole regions as compared to the polar coronal hole regions, this might have greater implications in the acceleration of the solar wind. But this fact has to be verified from a detailed statistical analysis done with several datasets, which we hope to pursue in near future. The details of the present study will be presented in O'Shea et al. (2005).

ACKNOWLEDGEMENTS

We would like to thank the CDS and EIT teams at Goddard Space Flight Center for their help in obtaining the present data. CDS and EIT are part of SoHO, the Solar and Heliospheric Observatory, which is a mission of international cooperation between ESA and NASA. Research at Armagh Observatory is grant-aided by the N. Ireland Dept. of Culture, Arts and Leisure. This work was supported by a PRTLI research grant for Grid-enabled Computational Physics of Natural Phenomena (Cosmogrid). We wish to thank the Royal Society and the British Council for funding visits between Armagh Observatory and the Indian Institute of Astrophysics. The original wavelet software was provided by C. Torrence and G. Compo, and is available at URL: http://paos.colorado.edu/research/wavelets/.

REFERENCES

1. Athay, R.G. & White, O.R., 1979, ApJ, 229, 1147

2. Banerjee, D., O'Shea, E. & Doyle, J.G., 2000, sol. phys, 196, 63

3. Banerjee, D., O'Shea, E., Doyle, J.G., Goossens, M., 2001a, A&A, 377, 691

4. Banerjee, D., O'Shea, E., Doyle, J.G., Goossens, M., 2001b, A&A, 380, L39

5. DeForest, C.E., Gurman, J.B., 1998, ApJ, 501, L217

6. Doyle, J.G., van den Oord, G.H.J., O'Shea, E., Banerjee, D., 1999, A&A, 347, 335

7. Harrison, R.A., Sawyer, E.C., Carter, M.K., Cruise, A.M. et al., 1995, sol. phys, 162, 233

8. Krieger, A. S., A. F. Timothy, and E. C., Sol. Phys., 29, 505-525, 1973

9. Munro, R. H., and G. L. Withbroe, Astrophys. J., 176, 511-520, 1972

10. Ofman, L., Romali, M., Poletto, G., Noci, G., & Kohl, J.L. 1997, ApJ, 491, L111

11. O'Shea, E., Banerjee, D., Doyle, J.G., Fleck, B., Mugtagh, F., 2001, A&A, 368, 1095

12. O'Shea, E., Banerjee, D., Doyle, J.G., 2005, A&A, (submitted)

13. Torrence, C., Compo, G.P., 1998, Bull. Amer. Meteor. Soc., 79, 61